Supplemental File 1: Additional theory and design considerations

Table of Contents

S1.1 Chemical diversity of modular rock-forming minerals 2

S1.2 Notation of module widths 4

S1.3 Design of TotBlocks 4

S1.4 Cleavage calculations 9

S1.5 An expanded dialogue on future work 10

S1.5.1 Crystal chemistry 10

S1.5.2 Other mineral structures 10

S1.5.3 Future design considerations 11

S1.6 A note on mineral nomenclature 11

S1.7 Supplemental videos 11

S1.8 References 12

S1.1 Chemical diversity of modular rock-forming minerals

Minerals that are based on *T* and *O* modules are diverse because many cations can be incorporated into their structures. To understand this diversity, it is necessary to determine which cations can be incorporated into which sites, focusing on the most abundant elements in the crust (Lide, 2005). We define four types of homologous cation sites within these minerals: (1) *T* sites, which reside in the *T* modules; (2) *M* sites, which reside in the *O* modules; (3) *B* sites, which border (flank) the *O* modules; and (4) *A* sites, which are commonly occupied by large alkali cations in inter-module spaces. For example, the *M*2 site in pyroxene-group minerals and the *B* site in amphibole-supergroup minerals both border the *O* modules, suggesting that these both belong to the *B* site grouping. Table 1 recasts the formulae of modular rock-forming minerals, classifying cation sites based on these four groups of homologous sites. The shapes of the *B* and *A* sites are more variable compared to *T* and *M* sites because their volumes depend on the configurations of the *T* and *O* modules.

Given that *T* and *O* modules form the common backbone of these minerals (Zoltai, 1981; Nespolo and Bouznari, 2017), the *T* and *M* sites will be discussed first, followed by the *B* and *A* sites. Goldschmidt's (1926, 1937) rules of substitution form the basis for determining whether elements can fit within a given site, as summarized below.

(1) Complete substitution occurs if the ionic radii of two elements differ by less than 15 %. Limited substitution exists if the difference is between 15–30 %.
(2) Ions whose charges differ by one unit substitute readily for one another, assuming charge neutrality is maintained. Limited substitution occurs if the charges differ by more than one unit.
(3) Substitution of the ion with higher ionic potential (charge divided by ionic radius) is preferred.

Oxygen and silicon are the most abundant elements in the crust, and the relative dimensions of their atomic radii lead to Si forming tetrahedrally coordinated complexes with oxygen (Lide, 2005; Pauling, 1929). Thus, *T* sites are dominantly occupied by Si, with an average Si–O bond distance of 1.62 Å (Smith and Bailey, 1963). Assuming idealized, planar sheets of regular, vertex-sharing Si–O tetrahedra sandwiching edge-sharing *M*–O octahedra (Fig. 1e–f), geometric calculations yield a theoretical *M*–O bond distance of 2.16 Å (Supplemental File 3). Subtracting the bond length of O^{2-} (1.36 Å; Shannon, 1976) gives a theoretical ionic radius of 0.80 Å for the *M* site. Thus, according to Goldschmidt's first rule, cations with ionic radii of 0.68–0.92 Å are expected to readily substitute into the theoretical *M* sites of these minerals. Using the homologous formulae of Table 1—with the assumption that *T* sites are fully occupied by Si^{4+}, *A* sites (and *B* sites in palygorskite-group minerals) are vacant, and *M* sites are fully occupied—yields average charges of 2+ for *M* and *B* sites for all modular rock-forming minerals. Thus, Goldschmidt's second rule suggests that cations with charges in the range of 1+ to 3+ should readily substitute into the *M* sites.

The ionic radii for the fifteen most-abundant elements in the earth's crust, along with the theoretically permissible bond distances of the *M* sites are shown in Fig. S1.1. It is apparent that Mg and Fe^{2+} (with lesser Mn^{2+}) exhibit complete solid solution within the *M* site. Conversely, Ca, Na, and K are too large for the *M* sites and are incorporated into the larger *B* and (even larger) *A* sites, which lie outside of the *T*-*O*-*T* modules (Morimoto et al., 1988; Hawthorne et al.,

2012; Rieder et al., 1998). Aluminum is a common constituent in the *M* sites of these minerals (Morimoto et al., 1988; Hawthorne et al., 2012; Rieder et al., 1998; Leung and McDonald, 2020), but Fig. S1.1 predicts that Al is too small to substitute in the *M* sites. This discrepancy can be explained by three reasons: (1) according to Goldschmidt's third rule, Al has a higher affinity for substitution because it has a higher ionic potential (smaller ionic radius and higher charge); (2) coupled substitution mechanisms for Al [e.g., ${}^{B}(Fe, Mg)^{2+} + {}^{M}(Fe, Mg)^{2+} \leftrightarrow {}^{B}Na^{+} + {}^{M}Al^{3+}$ in jadeite; Morimoto et al., 1988; and ${}^{M}(Fe, Mg)^{2+} + {}^{T}Si^{4+} \leftrightarrow {}^{M}Al^{3+} + {}^{T}Al^{3+}$ in the phengite series; Rieder et al., 1998] allow for greater flexibility in the crystal structure; and (3) the trioctahedral-to-dioctahedral substitution in *M* sites—most commonly $3(Fe, Mg)^{2+} \leftrightarrow 2Al^{3+} + \square$—leads to the distortion being accommodated by a larger, vacant *M* site (□).

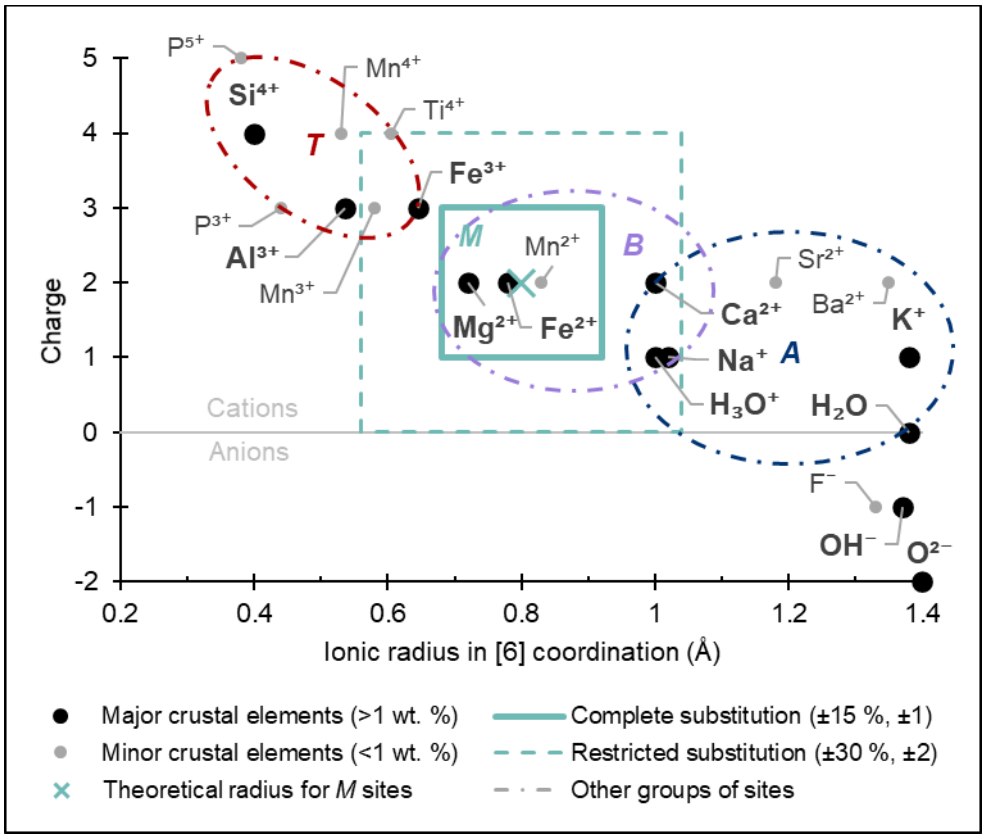

Fig. S1.1 Charge versus ionic radius scatter plot for the fifteen most-abundant elements in the crust in octahedral [6] coordination (Lide, 2005; Shannon, 1976; Marcus, 2013). The theoretical radius of *M* sites is shown, assuming ideally planar sheets of regular vertex-sharing silica tetrahedra joined to regular edge-sharing octahedra (Fig 1e–f in main text), along with areas bounded by solid lines denoting complete substitution and dashed lines denoting restricted substitution (following Goldschmidt, 1926; 1937). Regions within dot-dashed lines indicate the elements that may be found in other groups of crystallographic sites, in reference to Table 1 in the main text; note that these regions are approximate because the sites are of different coordination, and the ionic radii vary according to coordination.

Point (3) above additionally suggests that two distinct configurations exist for *O* modules: trioctahedral and dioctahedral structures. Trioctahedral members have a fully occupied *O* module (i.e., M_3), whereas in dioctahedral members, two-thirds of the *M* sites are occupied (i.e., $M_2\square$). The trioctahedral-dioctahedral division is found

throughout all layered modular minerals: brucite ≡ gibbsite (*O*); serpentine ≡ kaolinite (*T-O*); biotite series ≡ muscovite, beidellite ≡ saponite, talc ≡ pyrophyllite, (*T-O-T*), and clinochlore ≡ donbassite (*T-O-T O*).

In sum, the cations of the fifteen most-abundant elements in the earth's crust can fit into one of the four groups of crystallographic sites, which explains why these modular rock-forming minerals are abundant and chemically diverse in the crust (note that O, H, and F are readily incorporated into anionic sites within these structures; Fig. S1.1).

S1.2 Notation of module widths

The widths of the *T-O-T* rod modules can be expressed using two different notations (Fig. 2a).

(1) The simplest of these notations recognizes that the *T-O-T* rod modules are based on single-width chains (width $w = 1$, length $l = \infty$), double-width chains ($w = 2$, $l = \infty$), triple-width chains ($w = 3$, $l = \infty$), and infinite-width chains (i.e., sheets; $w = \infty$, $l = \infty$) of silica tetrahedra arranged in a *zweier* layout (Fig. 2a, top labels; modified after Zoltai, 1981; Liebau, 1985).
(2) Nespolo and Bouznari (2017) propose a more generalized notation based on the total number of sites (including multiplicity) present within a unit length of a *T* module ($T = 2,4,6\ldots$) and *O* module ($Z \approx 1,2,3\ldots$) (Fig. 2a, bottom labels). Although the *T* and *Z* notation proposed by Nespolo and Bouznari (2017) accounts for all widths of *T* and *O* modules that are theoretically possible, the notation is somewhat complicated.

The two notations are partially interchangeable for most crystal structures, i.e., $T = 2w$ and $Z \approx 3w - 1$, with few exceptions for *Z* values (e.g., kalifersite and, in a semantic sense, layered modular minerals; Table 1). For simplicity, we classify the module widths of biopyribole-palysepiole minerals using the first notation, i.e., based on the number of widthwise tetrahedral chains within the *T* modules ($w = 1, 2, 3, \ldots, \infty$). For reference, *Z* values which do not conform to $Z = 3w - 1$ will be listed for the corresponding crystal structures in the main text.

S1.3 Design of TotBlocks

The concept of modular, 3D-printed mineral-structure models was envisioned in the fall of 2019, when the lead author (DDVL) attempted to describe the crystal structure of a new mineral species to a non-specialist (his father). The species, windmountainite, is a member of the palygorskite group and its structure can be generally described as a hybrid between that of an amphibole and mica (Leung and McDonald, 2020). DDVL realized that, in his undergraduate mineralogy classes, many rock-forming minerals are described as being built from shared building blocks, but no attempts had been made to design physical versions of these building blocks. Reflecting on his undergraduate learning experience, DDVL also recalled that students commonly struggle with conceptualizing the crystal structures of minerals, due to the spatial aspects of the structures. As minerals form the basis for many geological disciplines (e.g., mineralogy, petrology, and structural geology), the struggle to recall mineral structures becomes a recurring issue in many geoscientists' careers. Hence, a physical teaching tool, rooted in modular mineralogy, could be useful for communicating mineral structures to general audiences, students, and researchers.

This idea, based in the lead author's experience of geology education and research, was subsequently actualized while exploring UCreate Studio, the makerspace at the University of Edinburgh.

The single-chain-width *T*-*O*-*T* rod module in Fig. 4d is broken down into *T* and *O* modules and their upside-down counterparts in Fig. S1.2a–b (compare T^+ versus T^-, O^+ versus O^-). The *T* modules are interchangeable, and thus it is the orientation of the apices of the *T* modules that defines the directionality of the *T* modules, rather than the specific modules themselves. On the other hand, the two types of *O* modules are not interchangeable and instead permit the construction of polytypes. Note that the + and − notation for *O* modules is reversed in this contribution when compared to Thompson's (1981) notation. This is because the + and − notation used in Thompson (1981) refers to the orientation of the stacking vector that is produced due to the lengthwise shifting of *T*-*O*-*T* modules, which is in the opposite orientation when considering the apices of the octahedra. Thompson (1981) did not distinguish between *T* modules at different orientations when investigating their stacking vectors. However, the orientations of the *T* modules are critical to understanding the resulting mineral linkages. The + and − notation for *T* modules is based on the orientation of the apex of the tetrahedron (Nespolo and Bouznari, 2017). For consistency among the *T* and *O* modules, we adopt the + and − notation based on the orientation (up and down, respectively) of the apices of the modules, when the widthwise pegs are facing rightward. Strictly speaking, the deviation from Thompson's (1981) notation is insignificant because the intent is to show opposing relative orientations, rather than the absolute orientations of the modules.

The *T* and *O* modules can be assembled into *T*-*O*-*T* rod modules using vertically oriented hexagonal pegs and slots. Conceptually, the hexagonal pegs and slots represent anions that are shared between the coordination polyhedra. The horizontally oriented hexagonal pegs and slots allow the *T*-*O*-*T* rod modules to connect lengthwise and widthwise via the three possible linkages (e.g., Fig. 2b–d). Using this linkage system, modules of different unit lengths and widths are compatible, provided that the scale of the template remains consistent. Modules of different widths and lengths can be generated from the 2:1 phyllosilicate template, such as single-chain-width (Fig. S1.2a–b), double-chain-width (Fig. S1.2c–d) and triple-chain-width (Fig. S1.2e–f) modules. For the layered minerals, extra octahedra are needed to fill missing *M* sites within the *O* modules (Fig. S1.3a), and vertical pegs of various lengths are used to vertically stack the individual sheets (Fig. S1.3b). Using the phyllosilicate-type linkage, multiple single-chain-width modules can be joined to make double-chain-width modules and so on, with extra octahedron pieces used to fill in missing sites within the *O* modules (Fig. S1.3a). For kalifersite, special Z_3 and Z_6 *O* modules are used (Fig. S1.4). Supplemental Video 2 contains an overview of each of the component pieces of TotBlocks, demonstrates how to assemble modules, and illustrates the different linkages between modules.

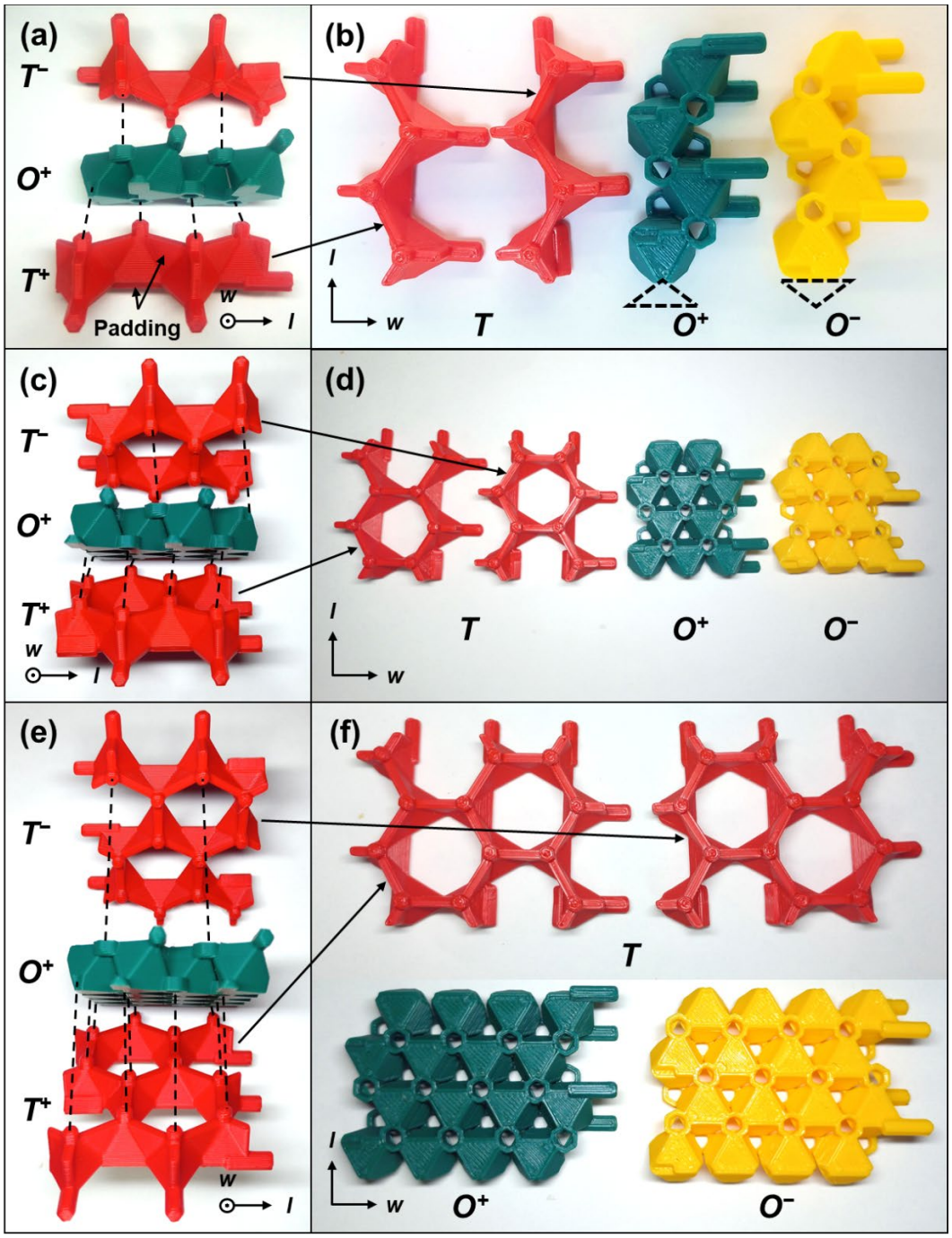

Fig. S1.2 (a) Disassembled single-chain-width ($w = 1$) *T-O-T* rod module, showing the component T^+, *O*, and T^- modules; dashed lines show hexagonal peg-and-slot linkages between the *T* and *O* rod modules. Padding of the *T* modules is labelled. (b) The four types of *T* and *O* modules ($w = 1$); dashed lines on the O^+ and O^- modules emphasize the opposite orientations of the two octahedra. (c) Disassembled and (d) individual component modules corresponding to double-chain-width ($w = 2$) *T-O-T* rod modules. (e) Disassembled and (f) individual component modules of triple-chain-width ($w = 3$) *T-O-T* rod modules. Note that the two variations of *T* modules are interchangeable, and the T^+ and T^- designation relates only to the direction that the apices of the *T* modules are pointing (up and down, respectively).

The accuracy of the crystal structures for the other layered minerals has not been quantitatively assessed in a manner such as that assessed for the biopyribole-palysepiole minerals by Nespolo and Bouznari (2017), and therefore the accuracy of these crystal-structure models can only be considered qualitatively. Additionally, some atomic sites (e.g., *B* and *A* sites) in the mineral structures are not part of the core *T*-*O*-*T* architecture and are less informative for the overall crystal structure. Thus, their presence detracts from commonalities among the different mineral groups. For these reasons, the sites were omitted from the design of TotBlocks. However, the positions of these sites are noted in the text and annotated as labelled circles in Figs. 6–7 following Nespolo and Bouznari (2017).

Since the *T* and *O* modules are separate, they can be printed in different colors using a basic single-extruder 3D printer to yield multi-colored *T*-*O*-*T* rod modules (e.g., Fig. 4d). Moreover, dual-extrusion 3D printers are useful for showing the crystal-chemical aspects of TotBlocks. For example, the *O* modules contain crystallographically distinct metal-oxygen (*M*) sites that can be occupied by different cations (e.g., Mg, Fe, and Mn), and the number and multiplicity of these sites depends on the unit width of the module. Thus, different colors can be used to differentiate between crystallographically distinct sites, which is aided by dual extrusion (Fig. S1.5a–c). This concept is less useful for the *T* modules because most of the *T* sites are occupied by Si (with lesser Al).

The design of the *T* modules is more problematic than the *O* modules because the tetrahedral chains are linked by the vertices, which is structurally weak and prone to breakage. This also poses a problem when forming T^{-}–T^{+} linkages because the *T* modules must be able to link to each other without extra supporting linkages from the *O* modules. Thus, padding was added to the *T* module to increase the strength and linking capability of the modules (Fig. S1.2a), but this obscures the true morphology of the *T* sites (compare Fig. 4a and c). The correct morphology of the *T* sites can be shown by using dual extrusion with translucent filament as padding (Fig. S1.5d). An example crystal structure (clinojimthompsonite; Veblen and Burnham, 1978a; 1978b) using the dual-extrusion version of TotBlocks is shown in Fig. S1.5e, which can be compared to the standard version in the main text (Fig. 6e).

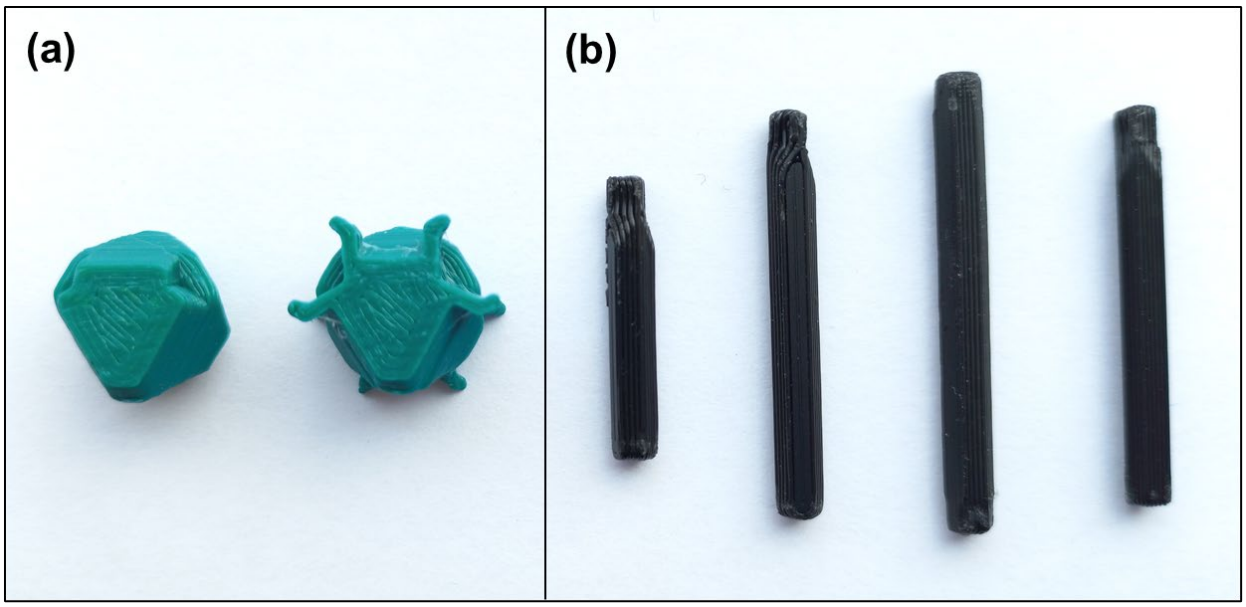

Fig. S1.3 Extra pieces used in TotBlocks. (a) Extra octahedron pieces without (left) and with (right) clips, which are used to fill in missing *M* sites when *T-O-T* modules are joined side by side (i.e., phyllosilicate-type linkages). The octahedra with clips are intended to be used when the additional octahedra are at the edges of the modules. (b) Vertical pegs, which are used to join parallel-lying sheets; note the different lengths corresponding to different layered minerals (left to right): brucite, kaolinite-serpentine (lizardite), mica, and chlorite groups.

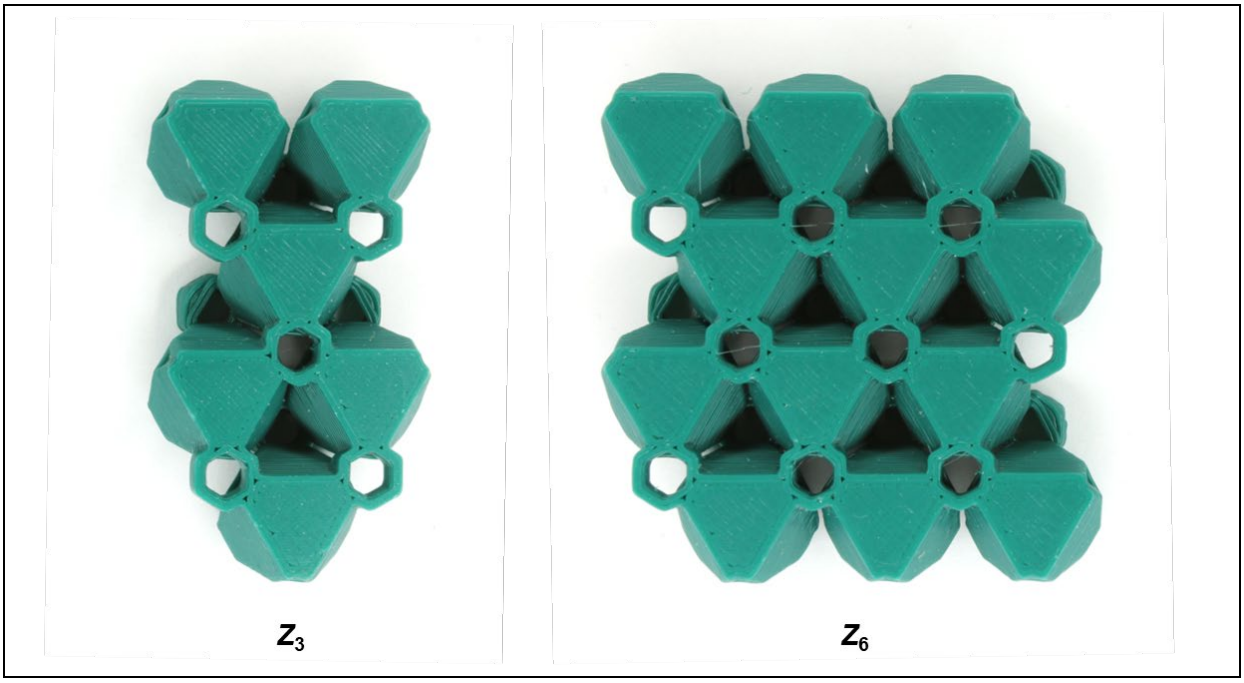

Fig. S1.4 Special Z_3 and Z_6 *O* modules used in the construction of kalifersite.

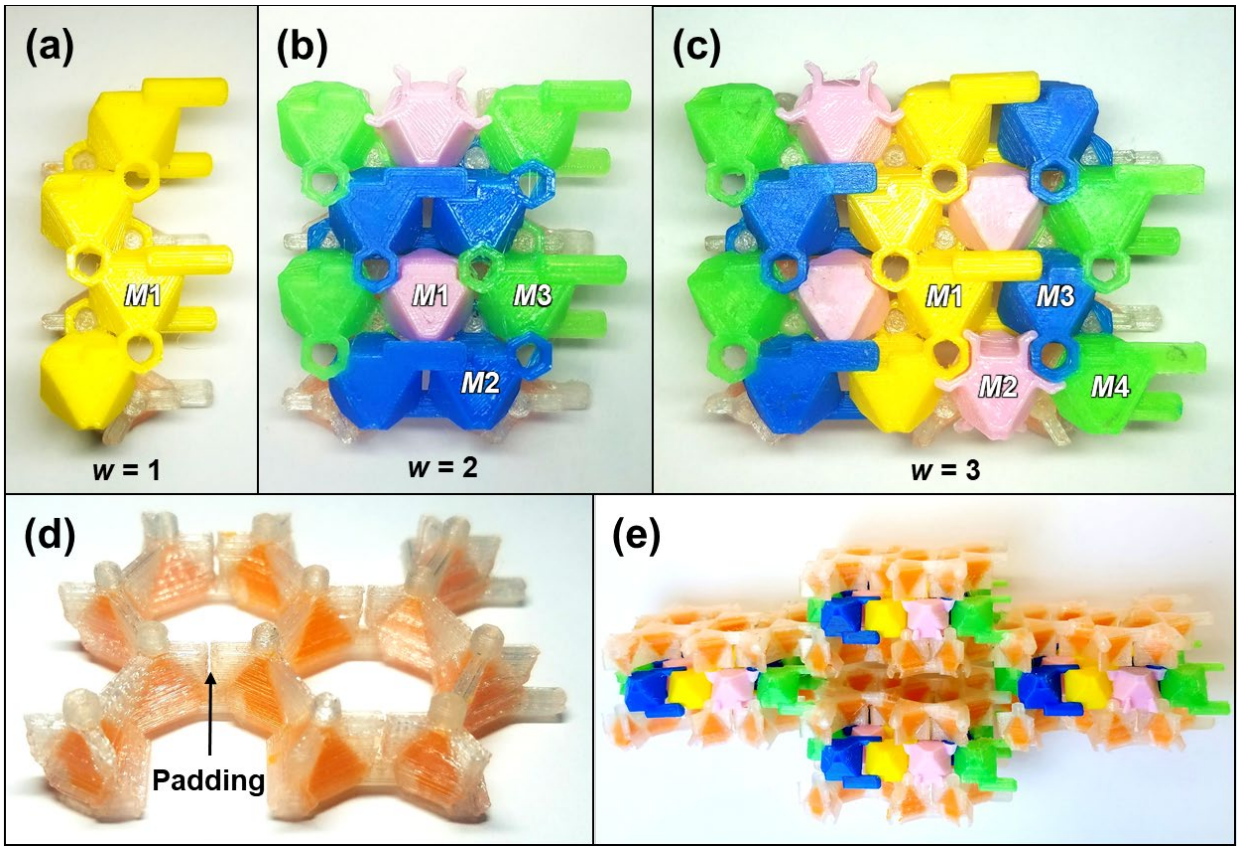

Fig. S1.5 (a)–(c) Multi-color version of TotBlocks, illustrating the crystallographically distinct *M* sites in the *O* modules for various module widths: (a) single- (*w* = 1), (b) double- (*w* = 2), and (c) triple-chain-width (*w* = 3) *T-O-T* rod modules. d) Multi-color version of *T* modules (*w* = 3) showing the true morphology of the *T* sites. Padding (labelled) is printed using translucent filament. (e) Example of multi-color version of TotBlocks (clinojimthompsonite, compare with main text; Veblen and Burnham, 1978a; 1978b).

S1.4 Cleavage calculations

The observed cleavage angles of the biopyriboles on the {110} (this cleavage is equivalent to {210} in orthopyribole polytypes *O2abc* because *a* is doubled for orthopyriboles) can be derived from first principles (Eq. S1.1), using trigonometry of the unit cell:

$$\theta_{obs} = 2\ \tan^{-1}(\frac{a}{b}); \tag{S1.1}$$

where θ and 180° - θ represent the two cleavage angles, and *a* and *b* are unit-cell dimensions of the mineral (height and width). (Note that for orthopyriboles, $\frac{a}{b}$ becomes $\frac{a}{2b}$ because *a* is doubled in orthopyriboles.) For example, the unit-cell dimensions for a member of the pyroxene group (*a* = 9.745 Å, *b* = 8.899 Å; Cameron et al., 1973) lead to almost perpendicular observed cleavage angles of ~85°/95° (Fig. 6a), whereas those for an amphibole (*a* = 9.51 Å, b = 18.19 Å; Fischer et al., 1966) suggest more divergent cleavage angles of ~125°/55° (Fig. 6d). A theoretical, infinite-width

($w = \infty$) pyribole loosely corresponds to the 2:1 phyllosilicate structure. These have one basal cleavage that could be considered as two degenerate cleavages at 180°/0°. Unsurprisingly, other layered minerals share the single basal cleavage displayed by the 2:1 phyllosilicates (Fig. 7d–f).

Using the concept of modular mineralogy, the cleavage angle can be approximated based on the module width (w) using Eq. S1.2:

$$\theta_{calc} = 2\tan^{-1}(w). \tag{S1.2}$$

In this way, the cleavage angle of chesterite ($w = 2.5$) is calculated to be 136°/44°, versus the observed 135°/45° (Veblen and Burnham, 1978a; Fig. 9a in the main text compares observed and calculated cleavage angles).

S1.5 An expanded dialogue on future work

S1.5.1 Crystal chemistry

TotBlocks can be used to investigate more advanced concepts such as the crystal chemistry of modular rock-forming minerals. Distinct *M* sites exist within the *O* modules, and these sites are homologous for minerals with equal module widths. The crystal chemistry of these minerals can be highlighted by distinguishing sites by color (Fig. S1.3a–c), and this is important because the mineral species are classified by the cations occupying these sites, either on an individual basis or as a whole (e.g., Leung and McDonald, 2020; Morimoto et al., 1988; Hawthorne et al., 2012).

S1.5.2 Other mineral structures

TotBlocks are currently restricted to a subset of rock-forming minerals (the biopyribole-palysepioles and other layered minerals). However, other minerals can be modeled with future work. Antigorite, $Mg_3Si_2O_5OH_4$, is a 1:1 phyllosilicate that is modulated lengthwise instead of widthwise, using variable-length *T* modules (*vierer* chains; Liebau, 1975; Capitani and Mellini, 2006). The structure of silinaite, $NaLiSi_2O_5{\cdot}2H_2O$, loosely resembles a $w = 1$ member of the palysepiole series, with edge-sharing Li tetrahedra replacing the *O* module (Grice, 1991). Pentagonite, $Ca(VO)Si_4O_{10}{\cdot}4H_2O$, loosely represents a lengthwise-modulated $l = 1$ analogue of the palysepiole series, with *T* modules consisting of *vierer* chains that sandwich zigzagging chains of alternating VO_5 and $CaO_4(H_2O)_3$ polyhedra (Evans, 1973; Liebau, 1975). Hexacelsian consists of T^+-T^- layer modules. See Day and Hawthorne (2020) and Hawthorne et al. (2019) for potential mineral structures or variants within the chain and sheet silicates, respectively. Non-modular structures that have repeating motifs can also be made, e.g., the 3_2 screw axes that make up the structure of quartz (Fig. S1.6).

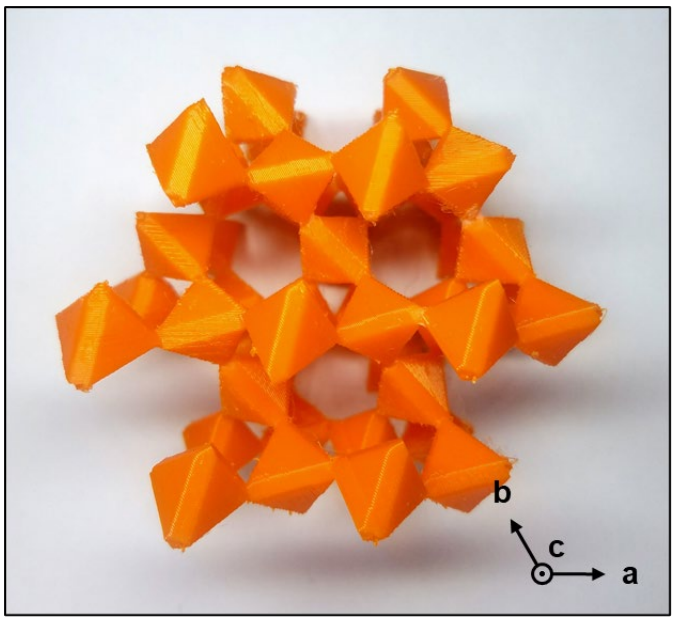

Fig. S1.6 A 3D-printed polyhedral model of hexagonal quartz (Kihara, 1990), consisting of seven 3_2 screw-axis modules that are glued together.

S1.5.3 Future design considerations

In future models, structural distortions may, in part, be accommodated with the use of flexible 3D-printing filament, whereas complex linkages may be simplified using ball magnets in conjunction with ferromagnetic 3D-printing filament. Caution should be taken when considering the crystallographic accuracy of these structures because compounding structural distortions and incompatible modules or linkages are more likely to pose a problem for increasingly complex series.

S1.6 A note on mineral nomenclature

We have chosen to use hierarchal nomenclature that has been established in the literature, despite a new standardization of mineral group hierarchies proposed by the International Mineralogical Association (Mills et al., 2009). We take this stance because the mineral group hierarchies have not been redefined for most biopyribole-palysepiole minerals, and such a redefinition is out of the scope of this contribution. Additionally, most undergraduate mineralogy courses are likely to retain the established hierarchal nomenclature.

S1.7 Supplemental videos

The titles of Supplemental Videos 1–13 are listed as follows:

(1) TotBlocks Video Abstract (https://doi.org/10.5446/57470; Leung and dePolo, 2022a),
(2) Assembly of TotBlocks (https://doi.org/10.5446/57471; Leung and dePolo, 2022b),

(3) 2:1 Phyllosilicates (https://doi.org/10.5446/57472; Leung and dePolo, 2022c),
(4) Pyroxene Group (https://doi.org/10.5446/57473; Leung and dePolo, 2022d),
(5) Amphibole Supergroup (https://doi.org/10.5446/57474; Leung and dePolo, 2022e),
(6) Clinojimthompsonite and Chesterite (https://doi.org/10.5446/57475; Leung and dePolo, 2022f),
(7) Palygorskite Group (https://doi.org/10.5446/57476; Leung and dePolo, 2022g),
(8) Sepiolite Group (https://doi.org/10.5446/57477; Leung and dePolo, 2022h),
(9) Kalifersite (https://doi.org/10.5446/57479; Leung and dePolo, 2022i),
(10) Brucite Group (https://doi.org/10.5446/57480; Leung and dePolo, 2022j),
(11) Kaolinite-Serpentine Group (https://doi.org/10.5446/57481; Leung and dePolo, 2022k),
(12) Chlorite Group (https://doi.org/10.5446/57482; Leung and dePolo, 2022l),
(13) How to 3D Print TotBlocks (https://doi.org/10.5446/57483; Leung and dePolo, 2022m).

S1.8 References

Cameron, M., Sueno, S., Prewitt, C. T., and Papike, J. J., High-temperature crystal chemistry of acmite, diopside, hedenbergite, jadeite, spodumene, and ureyite, Am. Min., 58(7–8), 594–618, 1973.

Capitani, G.C. and Mellini, M.: The crystal structure of a second antigorite polysome (m = 16), by single-crystal synchrotron diffraction, Am. Min., 91(2–3), 394–399, doi:10.2138/am.2006.1919, 2006.

Day, M. C. and Hawthorne, F. C.: A structure hierarchy for silicate minerals: Chain, ribbon, and tube silicates, Min. Mag., 84, 165–244, https://doi.org/10.1180/mgm.2020.13, 2020.

Evans, H. T.: The crystal structures of cavansite and pentagonite, Am. Min., 58(5–6), 412–424, 1973.

Fischer, K. F.: A further refinement of the crystal structure of cummingtonite, $(Mg,Fe)_7(Si_4O_{11})_2(OH)_2$, Am. Min., 51(5–6), 1966.

Goldschmidt, V. M.: The laws of crystal chemistry, Naturwissenschaften, 14, 477–485, 1926.

Goldschmidt, V. M.: The principles of distribution of chemical elements in minerals and rocks, J. Chem. Soc. Lond., 140, 655–673, 1937.

Grice, J. D.: The crystal structure of silinaite, $NaLiSi_2O_6 \cdot 2H_2O$: A monophyllosilicate, Can. Min., 29(2), 363–367, 1991.

Hawthorne, F. C., Oberti, R., Harlow, G. E., Maresch, W. V., Martin, R. F., Schumacher, J. C., and Welch, M. D.: Nomenclature of the amphibole supergroup, Am. Min., 97, 2031–2048, 2012.

Hawthorne, F. C., Uvarova, Y. A., and Sokolova, E.: A structure hierarchy for silicate minerals: sheet silicates, Min. Mag., 83, 3–55, https://doi.org/10.1180/mgm.2018.152, 2019.

Kihara, K.: An X-ray study of the temperature dependence of the quartz structure, Eur. J. Min., 2(1), 63–77, doi:10.1127/ejm/2/1/0063, 1990.

Leung, D. D. and McDonald, A. M.: Windmountainite, □Fe3+2Mg2Si8O20(OH)2(H2O)4·4H2O, a new modulated, layered Fe3+-Mg-silicate-hydrate from Wind Mountain, New Mexico: Characterisation and origin, with comments on the classification of palygorskite-group minerals, Can. Mineral., 58, 477-509, 2020.

Leung, D. D. V. and dePolo, P. E.: TotBlocks Video Abstract, TIB-AV Portal [video], https://doi.org/10.5446/57470, 2022a.

Leung, D. D. V. and dePolo, P. E.: Assembly of TotBlocks, TIB-AV Portal [video], https://doi.org/10.5446/57471, 2022b.

Leung, D. D. V. and dePolo, P. E.: 2:1 Phyllosilicates, TIB-AV Portal [video], https://doi.org/10.5446/57472, 2022c.

Leung, D. D. V. and dePolo, P. E.: Pyroxene Group, TIB-AV Portal [video], https://doi.org/10.5446/57473, 2022d.

Leung, D. D. V. and dePolo, P. E.: Amphibole Supergroup, TIB-AV Portal [video], https://doi.org/10.5446/57474, 2022e.

Leung, D. D. V. and dePolo, P. E.: Clinojimthompsonite and Chesterite, TIB-AV Portal [video], https://doi.org/10.5446/57475, 2022f.

Leung, D. D. V. and dePolo, P. E.: TotBlocks Palygorskite Group, TIB-AV Portal [video], https://doi.org/10.5446/57476, 2022g.

Leung, D. D. V. and dePolo, P. E.: Sepiolite Group, TIB-AV Portal [video], https://doi.org/10.5446/57477, 2022h.

Leung, D. D. V. and dePolo, P. E.: Kalifersite, TIB-AV Portal [video], https://doi.org/10.5446/57479, 2022i.

Leung, D. D. V. and dePolo, P. E.: Brucite Group, TIB-AV Portal [video], https://doi.org/10.5446/57480, 2022j.

Leung, D. D. V. and dePolo, P. E.: Kaolinite-Serpenting Group, TIB-AV Portal [video], https://doi.org/10.5446/57481, 2022k.

Leung, D. D. V. and dePolo, P. E.: Chlorite Group, TIB-AV Portal [video], https://doi.org/10.5446/57482, 2022l.

Leung, D. D. V. and dePolo, P. E.: How to 3D Print TotBlocks, TIB-AV Portal [video], https://doi.org/10.5446/57483, 2022m.

Lide, D. R.: CRC Handbook of Chemistry and Physics, 85th ed., CRC Press, 2005.

Liebau, F.: Crystal chemical classification of silicate anions, in: Structural Chemistry of Silicates: Structure, Bonding and Classification, Springer-Verlag, Berlin, Germany, 52–68, https://doi.org/10.1007/978-3-642-50076-3, 1985.

Marcus, Y.: Volumes of aqueous hydrogen and hydroxide ions at 0 to 200°C, J. Chem. Phys., 137(154501), 1–5, https://aip.scitation.org/doi/10.1063/1.4758071, 2013.

Mills, S. J., Hatert, F., Nickel, E. H., and Ferraris, G.: The standardization of mineral group hierarchies: Application to recent nomenclature proposals, Eur. J. Mineral., 21(5), 1073–1080, 2009.Morimoto, N., Fabries, J., Ferguson, A. K., Ginzburg, I. V., Ross, M., Seifert, F. A., Zussman, J., Aoki, K., and Gottardi, G.: Nomenclature of pyroxenes, Am. Min., 73, 1123–1133, 1988.

Morimoto, N., Fabries, J., Ferguson, A. K., Ginzburg, I. V., Ross, M., Seifert, F. A., Zussman, J., Aoki, K., and Gottardi, G.: Nomenclature of pyroxenes, Am. Min., 73, 1123–1133, 1988.

Nespolo, M. and Bouznari, K.: Modularity of crystal structures: a unifying model for the biopyribole-palysepiole series: Eur. J. Mineral., 29(3), 369-383, 2017.

Pauling, L.: The principles determining the structure of complex ionic crystals, J. Am. Chem. Soc., 51(4), 1010-1026, 1929.

Rieder, M., Cavazzini, G., D'Yakonov, Y. S., Frank-Kamenetskii, V.A., Gottardi, G., Guggenheim, S., Koval, P.V., Müller, G., Neiva, A.M.R., Radoslovich, E.W., Robert, J.-L., Sassi, F.P., Takeda, H., Weiss, Z., Wones, D.R.: Nomenclature of the micas, Can. Min., 36(3), 905–912, 1998.

Shannon, R.D.: Revised effective ionic radii and systematic studies of interatomic distances in halides and chalcogenides, Act. Cryst., A32, 751–767, 1976.

Smith, J.V. and Bailey, S.W.: Second review of Al–O and Si–O tetrahedral distances, Acta Cryst., 16, 801–811, doi:10.1107/s0365110x63002061, 1963.

Thompson, J. B.: An introduction to the mineralogy and petrology of the biopyriboles, Rev. Mineral. Geochem., 9A(1), 141–188, 1981.

Veblen, D. R. and Burnham, C. W.: New biopyriboles from Chester, Vermont: I. Descriptive mineralogy, Am. Mineral., 63, 1000-1009, 1978a.

Veblen, D. R. and Burnham, C. W.: New biopyriboles from Chester, Vermont: II. The crystal chemistry of jimthompsonite, clinojimthompsonite, and chesterite, and the amphibole-mica reaction, Am. Mineral., 63, 1053–1073, 1978b.

Zoltai, T.: Amphibole asbestos mineralogy, Rev. Mineral. Geochem., 9A(1), 237–278, 1981.